General Disclaimer

One or more of the Following Statements may affect this Document

- This document has been reproduced from the best copy furnished by the organizational source. It is being released in the interest of making available as much information as possible.

- This document may contain data, which exceeds the sheet parameters. It was furnished in this condition by the organizational source and is the best copy available.

- This document may contain tone-on-tone or color graphs, charts and/or pictures, which have been reproduced in black and white.

- This document is paginated as submitted by the original source.

- Portions of this document are not fully legible due to the historical nature of some of the material. However, it is the best reproduction available from the original submission.

Tcmp #42352

Solid Impingement Erosion Mechanisms and Characterization of Erosion Resistance of Ductile Metals

NOV 1983
RECEIVED
NASA STI FACILITY
ACCESS DEPT.

P. Veerabhadra Rao and Donald H. Buckley
Lewis Research Center
Cleveland, Ohio

NASA

SOLID IMPINGEMENT EROSION MECHANISMS AND CHARACTERIZATION

OF EROSION RESISTANCE OF DUCTILE METALS

P. Veerabhadra Rao[1] and Donald H. Buckley

National Aeronautics and Space Administration
Lewis Research Center
Cleveland, Ohio 44135

ABSTRACT

This paper presents experimental results pertaining to spherical glass bead and angular crushed glass particle impingement. A concept of energy absorption to explain the failure of material is proposed. The erosion characteristics of several pure metals were correlated with the proposed energy parameters and with other properties. Correlations of erosion and material properties were also carried out with these materials to study the effect of the angle of impingement. Analyses of extensive erosion data indicate that the properties - surface energy, strain energy, melting point, bulk modulus, hardness, ultimate resilience, atomic volume - and the product of the parameters - linear coefficient of thermal expansion x bulk modulus x temperature rise required for melting, and ultimate resilience x hardness - exhibit the best correlations. It appears that both energy and thermal properties contribute to the total erosion.

INTRODUCTION

The energy crisis and difficulties with nuclear power have forced many new power plants to use fossil fuel. This has caused severe erosion/corrosion problems and resulting SO_2 emissions have polluted the air. One piece of legislation now before Congress is the Clean Air Act (1983) which would regulate and control emissions. Physical cleaning of coal is the cheapest method of reducing sulfur emissions from the combustion process. The coal conversion, combustion and gasification processes lead to severe erosion problems in cyclones, piping, gasifiers, pumps, and valves. The energy conversion plants are expected to operate for more than 20 000 hours without a major shutdown. The high number of erosion related failures has, however, established erosion as a serious design consideration. The problems of component erosion due to particulate laden gases will continue to increase as system temperature and process speeds in various systems are increased. While coal gasification is one area

where erosion is a critical problem, there are other areas such as injection of debris into aircraft engines and particle impact on space vehicles which are also of major concern. A better understanding of basic processes and mechanisms involved in erosion is therefore of utmost importance.

Many attempts have been made to correlate the erosion rate of various ductile materials with their physical, mechanical, and other properties. However, no universal correlation using a single property or a combination of properties has been established. Table 1 presents the correlation attempts and suggestions made by different investigators [1 to 20] using a variety of properties. The particle geometry, sizes and shapes, the angle of impingement, and the velocity of impact are also recorded in the table.

Thus far, the different properties examined by various investigators have been: hardness [1, 3, 5, 8, 13, and 14], surface layer hardness [16], dynamic hardness [20], elastic modulus [2, 8, and 13], ductility [5, 8, 14, 16, and 20], localized ductility [19], melting temperature [6], tensile strength [8 and 14], yield stress [8 and 14], impact strength [14], fracture toughness [14], linear coefficient of expansion [14], product of hardness x elongation [1], 'thermal pressure' [7], product of density x specific heat x melting temperature differential [9], (mean molecular weight/density)$^{1/3}$ x (1/(thermal conductivity x melting temperature x enthalpy of melting)) [10], metal-metal bonding energy [11], ultimate resilience[2] [12], specific melting energy [15], cohesive energy [17], and strain energy[3] [18]. Pure physical properties of metals such as density [4] and specific gravity [8] have also been tried with nominal success. A majority of these investigators used erosion data reported either by Finnie, et al. [3] or Tadolder [21] or both.

From a physical understanding it is logical that the energy adsorbed by the material until it yields or

---

[1] Cleveland State University, Cleveland, Ohio 44115.

[2] Ultimate resilience = (tensile strength)^2/ [2 x elastic modulus].

[3] Work done to cause failure/unit volume and can be calculated from the area of the curve of an engineering stress-strain curve.

fails in a tension test is a simple property that is expected to roughly represent erosion resistance of ductile materials [22]. Although this type of correlation has recently been attempted [18] for pure metals using the data in reference [3], the correlations do not appear to be better than earlier attempts [7, 8, 10, 12, 14, 16, 18, and 19] using the same experimental data. Hence, an analysis of the energy absorption characteristics as well as melting due to the impinging particles and the experimental verification to assess the merit of the material properties in predicting erosion are necessary.

The mechanism of material removal during particle impingement has been attributed to extrusion, ductile fracture, melting, low-cycle fatigue, delamination, localized adiabatic shear, adhesive material transfer, and so forth [22]. Most of these postulations have resulted from wear debris and metallographic analyses. However, the platelet or flake-type wear debris observed on eroded material surfaces due to spherical particle impingement have not been observed for angular particle impingement. As shown in Figure 1 these phenomena have been named as deformation and cutting wear (with spherical and angular particle impact), respectively. The wear debris generation processes have been clearly illustrated in other papers as well [22 to 26].

More recently it has been made clear that two or three mechanisms can fully explain the erosion process with different shapes and sizes of particles [23 and 24]. Also, Brown and Edington [27] observed that material was lost via three different processes, namely, melting, dusting, and sheet formation. The micrographic observations in the literature [23, 25, and 27] and those of the present authors [22, 24, and 26] support the suggestion that the erosion process does not result from a single mechanism.

This paper assesses the erosion characteristics and mechanisms of pure metals to fully identify those properties best used for erosion prediction.

BACKGROUND OF MODELING EFFORTS

There have been several models proposed by different investigators for single and multiple spherical or angular particle impingement erosion. Excellent overviews of the subject have been presented by Ruff and Wiederhorn [28], Adler [29], Tilly [30], and Schmitt [31]. However, for completeness and to appraise the readers the models developed by various researchers are briefly highlighted. Finnie [32] in 1958 presented the dynamic equations governing the motion of the angular particle after it strikes the surface (using the concept of a rigid cutting tool removing a chip of material) considering the flow stress of material. This model has been modified later as discussed in references [29 and 33]. Bitter [34], categorizing deformation and cutting phenomena, developed an analytical equation based on an energy balance consideration of (1) recoverable elastic and elastic-plastic deformation energy and (2) nonrecoverable plastic deformation energy. Wood and Hafer [35] and Neilson and Gilchrist [36] have simplified the equations proposed by Bitter [34] to incorporate (1) the threshold normal velocity component and (2) the critical impingement angle of particles. The amounts of kinetic energy which have to be absorbed to remove a unit mass of material by cutting and deformation wear mechanisms have been discussed [36].

Mamoun [37] formulated a model to analytically predict material removal during spherical particle impingement using the Hertzian theory of contact and semi-empirical relationships pertaining to the fatigue life as a function of strain amplitude. He categorized the material response into six cases to consider his

prediction efforts for both ductile and brittle materials. Head and coworkers [10 and 38] proposed a model considering the energy transfer from (1) the impinging particles and (2) the nature of the response of the target, and the nature of the erosive media. Despite the fact that this model was developed for natural soils, it had a remarkable ability to predict particulate erosion because a parameter called modulus of toughness (similar to strain energy) was incorporated in the model. Tabakoff and his associates [39 and 40] have considered both particle trajectories and erosion in turbomachinery - gas turbine and compressor - components to model solid particle erosion using the statistical nature of the impact and the rebound characteristics. The intial model was fitted with small and large impingement angle dominant mechanisms. Further development and advances of their different models have recently been discussed by Tabakoff [40].

Hutchings, et al. [41] have contributed not only to an understanding of the individual mechanisms namely, plowing, cutting I and cutting II, but also to formulating a model based on the concept of a rigid sphere impacting normally on a rigid plastic plane. Later, Hutchings [20 and 42] presented a fatigue-type model using the concept of critical fracture strain to remove an elemental volume of the target material. This model produced useful results using the dynamic hardness and the ductility of the metal.

A "localization" model has recently been proposed by Sundararajan and Shewmon [43] using the critical plastic strain criteria defined as the strain which the deformation in the target localizes and hence results in the lip formation. The investigators contend that this model is superior to fatigue-type models and other models proposed thusfar because their model is able to demonstrate and explain the excellent correlation between the erosion rate and the "thermal pressure".

Although several other investigators made modeling efforts, it would be too time consuming to discuss all of these models in this paper.

MATERIALS, EXPERIMENTAL APPARATUS AND PROCEDURE

Materials

Specimens of copper, cobalt, nickel, indium, lead, and magnesium were used in this investigation. The specimens were 6 mm thick, 25 mm wide, and 37.5 mm long. Before exposure to erosion, all specimens were polished with 600-grit emery paper, then with 3 μm diamond paste, cleaned with distilled water, and air dried.

Apparatus and Procedure

A sandblasting facility was used to continuously impact test specimens at normal incidence. Commercial grade no. 9 spherical glass beads of 20 μm average diameter and commercial grade no. 10 crushed glass of 30 μm average size were used. The particle size distribution and SEM micrographic details of the glass beads have been presented by Rao, et al., [22, 24, and 26]. In the sandblasting facility the distance between the specimen and nozzle (1.18 mm diam) was 13 mm. Argon was used as the driving gas. The average jet velocity of the particles with both crushed glass and glass beads was 87 m/s. The velocities were measured by a double disk apparatus. The jet divergence was about 2° relative to the centerline and the glass bead and crushed glass flows were 0.89 and 0.22 g/s, respectively.

Profiles of the eroded surfaces were recorded with a profilometer and depths were measured with a depth gage. The eroded surfaces were observed with a scanning electron microscope (SEM) and chemical analyses

2

were obtained by means of energy dispersive X-ray spectroscopy (EDS).

EXPERIMENTAL OBSERVATIONS

Damage and Material Removal During Incubation Period

Figure 2 presents profilometer traces recorded on the pure copper specimen surface during glass bead and crushed glass impingement as a function of distance between the nozzle and the specimen, denoted in the figure by d. The experiments were conducted during incubation periods (2 s for crushed glass and 15 s for glass beads) for a particle jet velocity of 87 m/s. The profiles show two important aspects: (1) macroscopic flow of material during impingment and (2) 13 g of glass beads (Fig. 2(a)) induce more surface roughness than 0.44 g of crushed glass particles (Fig. 2(b)). These two observations support the suggestions that the flow of material, melting (on macroscopic level) and extrusion processes play important roles during the incubation period and the subsequent erosion process.

It is also evident from the traces in Figure 2 that strain hardening plays an important role as photographically shown in Figure 3. The weight loss[4] measurements of the specimens have not shown any loss of material. The surface traces in Figure 2 indicate a small material loss due to pit formation. This contradicting result may be attributed to two factors: (1) the embedment of particles and particle dust may be more than anticipated in earlier tests [22, 24, and 26] and (2) the strain hardening of the surfaces of materials as discussed in [43 and 44] may be extremely high so that the top thin layers of the material may be of higher density. Surface traces further explain the repeated extrusion and final low-cycle fatigue failure during glass bead impingement which is a manifestation of deformation wear. This is opposed to jagged, angular craters and cut surfaces with chips formed during cutting wear. These two mechanisms are photographically shown in Figures 1 and 2.

Material Loss and Energy Absorption

The concepts of thermal pressure [7], specific heat x density x temperature difference between the temperature of the metal and its melting point [9], ultimate resilience [12], specific melting energy (thermal energy density) [15], mechanical energy density[5] [18], and localization model [43] using critical plastic strain have contributed to an understanding of the erosion process and characterization of erosion resistance. However, the impinging spherical and angular particles as schematically shown in Figure 4 induce different deformation modes, namely, (1) elastic deformation, (2) plastic deformation, (3) plastic flow and lip formation, and (4) extrusion of material and melting (failure and splashing), resulting in material loss. Most of the time, the volume of the crater induced by an impact is not equal to the volume loss. This is due mainly to the fact that material deforms plastically and flows as a lip (Figs. 4(c) and (d)).

---

[4]Volume loss values were obatained by weighing specimens before and after their exposure to the erodents and dividing by density. The sensitivity of the balance was ±0.01 mg.

[5]This is also called the strain energy per unit volume of a material in a tensile test and approximately represents the area under the curve of an engineering stress-strain curve.

The Concept of Energy Absorption and Erosion

The volume loss measurement is an index of material erosion and it represents a part of total energy absorption efficiency of a material (to a first order of approximation) during solid particle impingement. Thus, the overall energy absorption efficiency η on the material surface may be defined as

$$\eta = \eta_{absorbed}/\eta_{impact}$$

$$= \text{erosion rate}/1/2 \ mV^{2p}f(\theta) \qquad (1)$$

$$\sim f(\text{material property})/1/2 \ mV^{2p}f(\theta) \qquad (2)$$

where m is the mean particle mass, V is the mean average particle velocity, p is the factor accounting for the velocity exponent deviations, and $f(\theta)$ is a factor representing scattering and angle of impingement, and size and shape of the particles. It is believed that only a part of the kinetic energy[6] from the impinging particles is absorbed by the surface of the material to cause damage and material removal. It was mentioned by Hutchings [20] that the energy balance during the particle impingement is as follows: 1 to 10 percent of the kinetic energy may rebound, 1 to 5 percent may be dissipated as elastic wave energy, and ~90 percent may be dissipated in plastic work (>80 percent heat and <10 percent stored energy).

Micrographs in Figure 2 and schematic failure modes in Figure 4 appear to indicate that energy absorption (along with thermal melting) plays a significant role. In order to investigate the energy absorption characteristics[7] and their relation to erosion, a simple relation of the following type is used:

Erosion rate

$$= A/f(\text{energy absorption property of material}) \qquad (3)$$

where A is a constant which depends on impact velocity, angle of impingement, and size, shape and concentration of particles. When a particle impinges on to a

---

[6]Erosive damage is sometimes a cumulative effect of series of impacts that do not individually produce any deformation visible under an optical microscope, but such impacts produce small increments of nucleation and expansion of dislocations in the crystalline structure surrounding the area of impact. These later interact to form cracks and eventually result in a low-cycle fatigue-type failure.

[7]A metal surface can store or absorb the kinetic energy of the solid particle in three different ways: (1) by elastic deformation, (2) by plastic deformation, and (3) by fracture. Figure 5 represents these three modes of energy absorption in a simple tensile test. Under these three modes the energy adsorption expressions can be calculated using proof resilience [(yield stress)^2/(2 x elastic modulus)], ultimate resilience [(tensile strength)^2/(2 x elastic modulus)] and strain energy (work done to cause failure = area under the stress-strain curve). The relative contributions of these parameters in determining damage depend upon the impact velocity, particle size, concentration, and shape, angle of impingement, and material properties (such as yield stress, ductility, tensile strength and elastic modulus). The erosion process depends upon the strain rate, contact time and area, local melting, deformation depth and area. The resulting erosion is thus a cumulative effect of all these factors.

surface, depending on the energy absorption of the material and considering the energy absorption modes in Figure 5 the following conditions exist resulting in different deformations:

condition (a) $0 \leq n_{abs} \frac{1}{2} mV^{2p} \leq P_R$ only elastic deformation

condition (b) $P_R \leq n_{abs} \frac{1}{2} mV^{2p} \leq U$ only plastic deformation

condition (c) $U \leq n_{abs} \frac{1}{2} mV^{2p} \leq Se$ failure only by fracture

where P_R is proof resilience ($= Y^2/2E$, U is the ultimate resilience ($= T^2/2E$), Se is the strain energy to failure ($= [(T + Y)El/2]$), Y is the yield strength, T is the tensile strength, E is the elastic modulus, and El is the percent elongation.

Based on the preceding information, equation (3) may be written as

$$\text{Erosion rate } A/(P_R, U, Se)^n \qquad (4)$$

In order to understand the dependence of the three energy absorbing parameters P_R, U, and Se on erosion rate, correlations were carried out using the relation in equation (3). Table 2 presents the statistical parameters obtained using the least-squares fit of the extensive erosion data reported earlier [3 and 21] including the data pertaining to the change of the angle of incidence. It is evident that correlations are good and more consistent with Se than with P_R and U at different particle velocities and angles of incidence. This intuitively indicates that complete failure of the material surface is a major factor contributing to the material loss. Ultimate resilience U is very good for certain sets only (Table 2). As mentioned earlier, volume loss is a part of the total damage to the surface. Hence, P_R and U play relatively less significant roles.

Attempts to correlate strain energy with erosion rate have been moderately successful [18 and 35]. Ultimate resilience was suggested by Eyre [12] for solid particle impingement erosion. The concepts of strain energy and ultimate resilience were originally proposed by Thiruvengadam [45] and Hobbs [46], respectively, for cavitation and liquid impingement erosion.

For certain groups of metals it is observed that

$$\text{Yield stress } Y \propto \text{hardness } H \qquad (5)$$

and

$$\text{Tensile strength } T \propto \text{hardness } H \qquad (6)$$

When some sets of the erosion data exhibited good correlations with hardness H, it is rather surprising that P_R ($= Y^2/2E$) and U ($= T^2/2E$) are not completely successful at high impingement angles ($30 \leq \theta \leq 90$). Hence, these correlations suggest that the erosion process is more complex than the pure energy absorption considerations, or than what was considered earlier.

In real situations, however, the following additional conditions may exist apart from conditions (a) to (c):

condition (d) $0 \leq n_{abs} \frac{1}{2} mV^{2p} \leq U$ elastic and plastic deformations

condition (e) $0 \leq n_{abs} \frac{1}{2} mV^{2p} \leq Se$ elastic and plastic deformations and fracture

condition (f) $n_{abs} \frac{1}{2} mV^{2p} \geq Se$ complete ductile fracture

In view of this, it may be advisable to consider a relation similar to

$$\text{Erosion rate} = 1 \Big/ \left(A_1 P_R^{n1} + A_2 U^{n2} + A_3 Se^{n3} \right) \qquad (7)$$

or

$$\text{Erosion rate} = A \Big/ \left(P_R^{n1} + U^{n2} + Se^{n3} \right) \qquad (8)$$

in order to fully understand the extent of elastic, plastic and failure energies involved in the erosion process and the relation between local melting and ductile failure at different velocities of impact, angle of impingement, and sizes and shapes of particles.

Other Material Property Correlations

The main purpose of correlations is to characterize the erosion resistance of various metals with some other property. Most of the time, it is necessary that the material property should exhibit all the complex processes involved in erosion, yet be simple and straightforward in order to be used by design engineers.

Table 3 presents statistical parameters obtained for the correlation of the extensive erosion data [3 and 21] with various properties.[8] The properties considered are surface energy, yield stress, tensile strength, density, hardness, melting point, elastic modulus, bulk modulus, acoustic impedence, coefficient of expansion, cohesive energy, atomic volume, metal-metal bond energy, $C_p \rho \Delta T$, $\alpha K \Delta T$, ultimate resilience x hardness, and (Debye temperature)^2 x atomic weight. The majority of properties were obtained from reference [47].[8] Data pertaining to different angles of impingement are also presented in this table.

With single properties, surface energy, melting point, bulk modulus, strain energy, hardness, and atomic volume are good for correlating erosion rates of metals (Tables 2 and 3). The properties, bulk modulus and ultimate resilience, become less signficant as the angle of impingement reaches 90°. However, surface energy, atomic volume, Se, and hardness seem to be better even at this impingement condition than the other properties.

Figures 6 to 8 present typical plots of the erosion rate of several metals as a function of surface

---

[8]The properties of metals obtained depend on (1) the purity of the metal, (2) the surface treatment used, (3) the type of device employed, and (4) the method adopted for evaluation. Hence, it is necessary to assess metal properties more precisely.

energy, atomic volume, and melting point. These fig-
ures show the permissible data scatter and the good
correlation characteristics. The least-square lines
of the curve fit for 30°, 50°, and 90° angle impinge-
ment were only the ones plotted omitting the data
points. The data obtained by the present authors and
others [4, 8, 48, and 49] are also presented. The good
correlation with melting point (Fig. 8) and strain en-
ergy (Tables 2 and 3) support the experimental obser-
vation of possible melting and flow of the material
surface in Figure 2.

When considering multiple properties, thermal
pressure ($\alpha K_\Delta T$), ultimate resilience x hardness, (Debye
temperature)^2 x atomic weight and $C_p \rho_\Delta T$ are listed
in decreasing order of merit. There is good correla-
tion with thermal pressure compared to other properties
even at normal incidence.

Figure 9 presents a typical plot of erosion rate
as a function of thermal pressure. It is to be remem-
bered that "thermal pressure" contains both bulk modu-
lus and melting point (which are good correlating
single properties to represent erosion). Ultimate re-
silience x hardness is not much superior to ultimate
resilience and hardness considered individually.

From the good correlation of properties of mate-
rials, the following inferences can be made: (1) the
erosion process is either (fracture) strain energy or
thermal energy related resulting in ductile tearing or
a local melting process; (2) the energy absorption
capability of the material surface is always related to
the erosion process. At this juncture it is logical to
assume that both fracture and thermal energy properties
are interrelated during the complex erosion process.
The melting point [6] and specific melting energy [15]
have been successfully correlated with erosion.

The good correlation of erosion rate with atomic
volume indicated that the damage process is submicro-
scopic in nature. The generation of wear debris is a
concerted effort of both mechanical and thermal energy
interaction resulting in gross damage and material
loss.

Erosion Resistance

It is generally observed that the erosion rates of
different metals from Bi to W vary by two orders of
magnitude. Most of the properties such as cohesive en-
ergy, metal-metal bond energy including surface energy,
melting point, atomic volume, and bulk modulus vary
only by one order of magnitude. Despite this fact sur-
face energy and atomic volume are better correlating
properties than cohesive energy, metal-metal bond en-
ergy, density, linear coefficient of thermal expansion,
and $C_p \rho_\Delta T$. It is, in general, observed that proper-
ties of materials from Bi to W not varying at least
over two orders of magnitude may not appear to be good
for correlation purposes to represent a wide spectrum
of metals.

On the other hand, hardness, ultimate resilience,
strain energy, and $\alpha K_\Delta T$ vary approximately over two
orders of magnitude. Hence, these parameters along
with surface energy and atomic volume may be better
properties to represent the erosion resistance of a
wide spectrum of metals.

Discrepancies in Earlier Correlations

The different property correlations proposed by
earlier investigators [1 to 18] are not in agreement.
The main reasons for the disagreement are the following:
(1) most of the earlier investigators used erosion data
at 20° incidence [3] (A detailed statistical analysis
as presented here clearly shows the importance of var-
ious properties as the angle of impingement changes.),

(2) data for pure metals and alloys were not separated,
(3) material properties except hardness were not ob-
tained at the time of testing, (4) the majority of cor-
relation studies were done with angular particles (in
which cutting wear predominates) except by Jennings,
et al. [10] and the present investigators, (5) some
metals for example, Bi and W, exhibited brittle-type
metal failure similar to glass [3] instead of ductile-
type failure, and (6) the entire spectrum of materials
were not considered. The groupings of metals tested
by various investigators were different.

Exponents and Coefficients

In order to predict the erosion characteristics of
untested metals with the following known equation, both
A and n are necessary:

$$\text{Erosion rate} = A/(\text{material parameter})^n$$

It is evident from Tables 2 and 3 that exponents in-
creased as the angle of impingement increases. How-
ever, the values obtained are fairly constant and agree
well with the two sets of data used [3 and 21]. Hence,
it may be stated that the variables such as angle of
impingement, size and shape of particles and impact
velocity do not seem to influence the exponent values.

The values of coefficients decrease as the value
of impingement increases from peak erosion (15° to 30°)
to normal incidence (90°). Limited studies indicate
that the coefficient appears to vary as $(\sin\theta_m/\sin\theta)^m$, (m varying between 1 and 2), with the
angle of impingement. The coefficients vary as V^{2p}
with the impact velocity. The value of p is avail-
able from the parametric studies and generally varies
between 1 and 7/4.

CONCLUSIONS

1. Both surface traces and SEM micrographs demon-
strated plastic flow and melting on the material sur-
face during impingement with spherical and angular
particles.

2. Energy absorption characteristics do not fully
represent the erosion behavior of a metal.

3. Analyses of extensive erosion data indicate
that surface energy, strain energy, atomic volume,
melting point, bulk modulus, hardness, and ultimate
resilience exhibit good correlations with erosion.
However, only surface energy, atomic volume, and
strain energy provide good correlations at different
angles of impingement. In product parameters, coeffi-
cient of thermal expansion x bulk modulus x melting
point differential ($\alpha K_\Delta T$) is found to be the best pa-
rameter for correlations with erosion rate followed by
ultimate resilience x hardness, and (Debye tempera-
ture)^2 x atomic weight.

4. The exponential values in the present studies
are consistent. The coefficients generally appear to
vary as $V^{2p}(\sin\theta_m/\sin\theta)^m$ with impact velocity V
and angle of impingement θ. In this $1 \le m \le 2$ and
$1 \le p \le 3/4$.

REFERENCES

1. Wood, C. D., and Espenschade, P. W., "Mechanisms
   of Dust Erosion," SAE Transactions, Vol. 73, 1965,
   pp. 515-523.
2. Brauer, H., and Kriegel, E., "Verschleiss von
   Rohrkrummern beim pneumatischen und hydraulischen
   Feststofftransport (Erosion of Pipe Bends in Pneu-
   matic and Hydraulic Solids - Transport)," Chemie.
   Ingenieur Tech, Vol. 37, 1965, pp. 265-276.

3. Finnie, I., Wolak, J., and Kabil, Y., "Erosion of Metals by Solid Particles," Journal of Materials, Vol. 2, No. 3, Sept. 1967, pp. 682-700.

4. Kayser, W., "Erosion by Solid Bodies," Proceedings of 2nd Meersburg Conference on Rain Erosion and Allied Phenomena, A. A. Fyall and R. B. King, eds., Royal Aircraft Establishment, Farnborough, England, 1967, pp. 427-447.

5. Tilly, G. P., "Erosion caused by Airborne Particles," Wear, Vol. 14, July 1969, pp. 63-79.

6. Smeltzer, C. E., Gulden, M. E., and Compton, W. A., "Mechanisms of Metal Removal by Impacting Dust Particles," Journal of Basic Engineering, Vol. 92, No. 3, Sept. 1970, pp. 639-654.

7. Ascarelli, P., "Relation between the Erosion by Solid Particles and the Physical Properties of Metals," AMMRC-TR-71-47, Army Materials and Mechanics Research Center, Watertown, Massachusetts, Nov. 1971. (AD-738162.).

8. Tuitt, D. A., "Erosion Tests of Metallic Coatings", Proceedings of 4th International Conference on Rain Erosion, A. A. Fyall and R. B. King, eds., Royal Aircraft Establishment, Farnborough, England, 1974, pp. 677-699.

9. Hutchings, I. M., "Prediction of the Resistance of Metals to Erosion by Solid Particles," Wear, Vol. 35, 1975, pp. 371-374.

10. Jennings, W. H., Head, W. J., and Mannings, C. R., "A Mechanistics Model for the Prediction of Ductile Erosion," Wear, Vol. 40, No. 1, Oct. 1976, pp. 93-112.

11. Vijh, A. K., "Resistance of Metals to Erosion by Solid Particles in Relation to the Solid State Cohesion of Metals," Wear, Vol. 39, No. 1, Aug. 1976, pp. 173-175.

12. Eyre, T. S., "Wear Characteristics of Metals." Tribology International, Vol. 9, No. 5, Oct. 1976, pp. 203-212.

13. Sheldon, G. L., "Effects of Surface Hardness and Other Material Properties on Erosive Wear of Metals by Solid Particles," Journal of Engineering Materials and Technology, Vol. 99, No. 2, Apr. 1977, pp. 133-137.

14. Jones, M. H., and Lewis, R., "Solid Particle Erosion of a Selection of Alloy Steels," Proceedings of 5th International Conference on Erosion by Solid and Liquid Impact, Cambridge University, Cambridge, England, 1979, Paper 52.

15. Malkin, S., "Correlation between Solid Particle Erosion of Metals and Their Melting Energies," Wear, Vol. 68, No. 3, May 1981, pp. 391-396.

16. Söderberg, S., Hogmark, S., and Swahan, H., "Mechanisms of Material Removal During Erosion of a Stainless Steel," ASLE Transactions, Vol. 26, No. 2, Apr. 1983, pp. 161-172.

17. Buckley, D. H., "Importance and Definition of Materials in Tribology," International Tribology Conference, NASA Lewis Research Center, Apr. 18-21, 1983.

18. Rickerby, D. G., "Correlation of Erosion with Mechanical Properties in Metals," Wear, Vol. 84, No. 3, Feb. 1983, pp. 393-395.

19. Levy, A. V., "The Role of Plasticity in Erosion," Proceedings of 5th International Conference on Erosion by Solid and Liquid Impact, Cambridge University, Cambridge, England, 1979, Paper 39.

20. Hutchings, I. M., "A Model for the Erosion of Metals by Spherical Particles at Normal Incidence," Wear, Vol. 70, No. 3, Aug. 1981, pp. 269-281.

21. Tadolder, Y. A., "Influence of Abrasive Grain Geometry on the Solid Particle Erosion of Metals," Tr. Tallin Politekh Inst., Series A., Vol. 237, 1966, pp. 15-22.

22. Rao, P. V., Young, S. G., and Buckley, D. H., "A Study of the Nature of Solid Particle Impact and Shape on the Erosion Morphology of Ductile Metals," NASA TM-82933, July 1982.

23. Finnie, I., Levy, A., and McFadden, D. H., "Fundamental Mechanisms of the Erosive Wear of Ductile Metals by Solid Particles," Erosion: Prevention and Useful Applications, W. F. Adler, ed., ASTM STP 664, American Society for Testing and Materials, Philadelphia, PA., 1979, pp. 36-58.

24. Rao, P. V., Young, S. G., and Buckley, D. H., "Morphology of Ductile Metals Eroded by a Jet of Spherical Particles Impinging at Normal Incidence," Wear, Vol. 85, No. 1, Mar. 1983, pp. 223-227.

25. Ruff, A. W., "Debris Analysis of Erosive and Abrasive Wear", Fundamentals of Tribology, N. P. Suh and N. Saka, eds., MIT Press, Cambridge, Mass., 1980, pp. 877-885.

26. Rao, P. V., Young, S. G., and Buckley, D. H., "Morphology of an Aluminum Alloy Eroded by a Jet of Angular Particles Impinging at Normal Incidence," NASA TP 2139, May 1983.

27. Brown, R., and Edington, J. W., "Mechanisms of Material Loss During the Threshold Period of Erosion by Solid Particles", Wear, Vol. 77, No. 3, Apr. 1982, pp. 347-353.

28. Ruff, A. W. and Wiederhorn, S. M., "Erosion by Solid Particle Impact," Treatise on Materials Science and Technology, Vol. 16, Materials Erosion, C. M. Preece, ed., New York, Academic Press, 1979, pp. 69-126.

29. Adler, W. F., "Assessment of the State of Knowledge Pertaining to Solid Particle Erosion," ETI CR 79-680, Effects Technology, Inc., Santa Barbara, Calif., June 1979 (AD-AO73034.)

30. Tilly, G. P., "Erosion by Impact of Solid Particles," Treatise on Materials Science and Technology, Vol. 13, D. Scott, ed., Academic Press, New York, pp. 287-319.

31. Schmitt, G. F., Jr., "Liquid and Solid Particle Impact Erosion," Wear Control Handbook, M. B. Peterson and W. O. Winer, eds., American Society of Mechanical Engineers, New York, 1980, pp. 231-282.

32. Finnie, I., "The Mechanism of Erosion of Ductile Metals," Proceedings 3rd National Congress on Applied Mechanics, American Society of Mechanical Engineers, New York, 1958, pp. 527-532; see also "Erosion of Surfaces by Solid Particles," Wear, Vol. 3, 1960, pp. 87-103.

33. Finnie, I., Levy, A., and McFadden, D. H., "Fundamental Mechanisms of the Erosive Wear of Ductile Metals by Solid Particles," Erosion: Prevention and Useful Applications, ASTM STP 664, W. F. Adler, ed., American Society for Testing and Materials, Philadelphia, 1979, pp. 36-58.

34. Bitter, J. G. A., "A Study of Erosion Phenomena, Parts I and II," Wear, Vol. 6, 1963, pp. 5-21 and 169-190.

35. Wood, C. D. and Hafer, C. A., "Dust Research Studies," AR-572, Southwest Research Institute, San Antonio, Texas, Feb. 1966.

36. Neilson, J. H. and Gilchrist, A., "Erosion by a Stream of Solid Particles," Wear, Vol. 11, 1969, pp. 111-122.

37. Mamoun, M., "Analytical Models for the Erosive-Corrosive Wear Process," Rept. ANL-75-XX-2, 1975, Appendix I, Argonne National Laboratory, Ill., 1975.

38. Head, W. J. and Harr, M. E., "The Development of a Model to Predict the Erosion of Materials by Natural Contaminants,: Wear, Vol. 15, 1970, pp. 1-46; Head, W. J., Lineback, L. D., and Manning, C. R., "Modification and Extension of a Model for Predicting the Erosion of Ductile Materials," Wear, Vol. 23, 1973, pp. 291-298.

39. Grant, G. and Tabakoff, W., "Erosion Prediction in Turbomachinery Resulting from Environmental Solid Particles," Journal of Aircraft, Vol. 12, No. 5, May 1975, pp. 471-478; Kotwal, R. and Tabakoff, W., "A New Approach for Erosion Prediction Due to Fly Ash," Journal of Engineering for Power, Vol. 103, No. 2, Apr. 1981, pp. 265-270.

40. Tabakoff, W., "Performance Deterioration on Turbomachinery with Presence of Solid Particles," Particulate Laden Flows in Turbomachinery, W. Tabakoff, C. T. Crowe, and D. B. Cale, eds., American Society of Mechanical Engineers, New York, 1982, pp. 3-22.

41. Hutchings, I. M., Winter, R. E., and Field, J. E., "Solid Particle Erosion of Metals: The Removal of Surface Material by Spherical Projectiles," Proceedings, Royal Society, London, Series A, Vol. 348, No. 1654, Mar. 9, 1976, pp. 379-392; Hutchings, I. M., "Mechanisms of the Erosion of Metals by Solid Particles,: Erosion: Prevention and Useful Applications, ASTM STP 664, W. F. Adler, ed., American Society for Testing and Materials, Philadelphia, 1979, pp. 59-76.

42. Hutchings, I. M., "Some Comments on the Theoretical Treatment of Erosive Particle Impacts." Proceedings of 5th International Conference on Erosion by Solid and Liquid Impact, Cambridge University, Cambridge, England, 1979, Paper 36.

43. Sundararajan, G. and Shewmon, P. G., "A New model for the Erosion of Metals at Normal Incidence," Wear, Vol. 84, No. 2, Jan. 1983, pp. 237-258.

44. Cousens, A. K. and Hutchings, I. M., "A Critical Study of the Erosion of an Aluminum Alloy by Solid Spherical Particles at Normal Impingement," Wear of Materials, 1983, K. C. Ludema, ed., American Society of Mechanical Engineers, New York, 1983, pp. 382-389.

45. Thiruvengadam, A., "A Unified Theory of Cavitation Damage," Journal of Basic Engineering, Vol. 85, No. 3, Sept. 1963, pp. 365-376.

46. Hobbs, J. M., "Experience with a 20-kc Cavitation Erosion Test," Erosion by Cavitation or Impingement, ASTM STP 408, American Society for Testing and Materials, Philadelphia, 1967, pp. 157-185.

47. Gschneidner, Jr., K.A., "Physical Properties and Interrelationships of Metallic and Semimetallic Elements," Solid State Physics, Advances in Research and Applications, F. Seitz and D. Turnbull, eds., Academic Press. New York, Vol. 16, 1964, pp. 276-426.

48. Hansen, J. S., "Relative Erosion Resistance of Several Materials," Erosion: Prevention and Useful Applications, A. F. Adler, ed., ASTM STP 664, American Society for Testing and Materials, Philadelphia, 1979, pp. 148-162.

49. Söderberg, S., Hogmark, S., Engman, U., and Swahan, H., "Erosion Classification of Materials Using a Centrifugal Erosion Tester." Tribology International, Vol. 14, No. 6, Dec. 1981, pp. 323-343.

TABLE 1. - MATERIAL PROPERTY CORRELATIONS WITH SOLID PARTICLE IMPINGEMENT EROSION

Investigator	Erosion parameter	Correlated or suggested properties of materials	Angle of impingement, deg	Particle velocity, m/s	Impinging particles (size, μm)
Wood and Espenschade [1][a]	Erosion rate	Hardness (Knoop) Hardness x elongation	90	[b]225	Silica flour (74)
Brauer and Kriegel [2]	Erosion	Elastic modulus	-----	-----	--------
Finnie, et al. [3]	Volume removed	Hardness (VHN)	20	76,137	SiC (250)
Kayser [4]	Resistance to erosion	Density (metals, alloys, and plastics)	-----	143	Quartz sand (400)
Tilly [5][F]	Erosion	Hardness (VHN), ductility at fracture	90	104	Quartz (60-125)
Smeltzer, et al. [6][d]	Volume removed.	Melting temperature	20	137	SiC (250)
Ascarelli [7][d]	Volume eroded	Thermal pressure (product of linear thermal expansion, temperature rise required for melting, and bulk modulus of metal)	20	137	SiC (250)
Tuitt [8][F]	Volume loss	Hardness, tensile strength, ductility, proof stress, specific gravity, elastic modulus	30,90	305	Quartz sand (40)
Hutchings [9][d],[f]	Volume loss rate	Density x specific heat x temperature rise required for melting	20 45	137 82	SiC (250) Quartz
Jennings et al. [10][g]	Volume loss	$\dfrac{(\text{Mean molecular weight/density})^{1/3}}{(\text{Thermal conductivity} \times \text{melting temperature} \times \text{enthalpy of melting})}$	20,30,45, 90	91-253	Glass beads (%00) SiC (220)
Vijh [11][d],[f]	Wear resistance	Metal-metal (interatomic) bond energy	20 45	137 82	SiC (250) Quartz
Eyre [12]	Erosion	Ultimate resilience (tensile strength^2/(2 x elastic modulus))	-----	-----	--------
Sheldon [13][d],[h]	Erosion wear	Hardness (VHN), elastic modulus	20	76	SiC (250)
Jones and Lewis [14][F]	Erosion wear rate	Impact strength, ultimate tensile strength, fracture toughness, elongation, hardness, coefficient of thermal expansion	90	-----	Quartz SiC Iron powder
Malkin [15][d],[f]	Specific erosion energy[i]	Specific melting energy (melting energy per unit volume of target)	20 45	76,137 82	SiC (250) Quartz
Söderberg, et al. [16]	Cutting erosion resistance	Surface layer hardness	15,30,45, 60,75,90	20,66, 100	Olivine sand (350-490)
	Deformation erosion resistance	Ductility	15,30,45, 60,75,90	20,66, 100	Olivine sand (350-490)
Buckley [17][d]	Weight loss rate	Cohesive energy	20	137	SiC (250)
Rickerby [18][F]	Volume erosion	Mechanical energy density (strain energy)	20	76,137	SiC (250)
Levy [19]	Erosion resistance	Localized ductility	15,30,90	30,61	SiC (240)
Hutchings [20]	Erosion resistance	Dynamic hardness and ductility	90	30-75	Glass beads (212-250 and 495-600) Steel shot (600-700)

a Several steels were correlated.
b Airstream velocity (particle velocity is much smaller than this value).
c Several alloys were correlated.
d Finnie, et al. [3] data have been adopted.
e Erosion resistance of several alloys and coatings were correlated.
f Tadolder [21] data have been adopted.
g Seven alloys were correlated.
h Apart from pure metals, Cu-Ni alloys were also correlated.
i Kinetic energy per unit volume of target material (using an analogy with grinding).

TABLE 2. - CORRELATIONS OF ENERGY PROPERTIES WITH EROSION*

[Erosion rate = $A/(P_R, U, Se)^n$. P_R = proof resilience = $Y^2/2E$; U - ultimate resilience = $T^2/2E$;
Se = strain energy = $(T + Y)El/2$; Y = yield stress; T = tensile strength; F = elastic modulus;
El = elongation; V = particle velocity; θ = angle of impingement.]

Energy property	Correlation parameter	Tadolder [21] data; quartz sand; $V = 82$ m/s; $\theta = 45°$	Finnie, et al. [3] data; SiC (250 μm size)				
			$V = 136$ m/s; $\theta = 20°$	$V = 76$ m/s; $\theta = 20°$	$V = 76$ m/s; $\theta = 30°$	$V = 76$ m/s; $\theta = 50°$	$V = 76$ m/s; $\theta = 90°$
Proof resilience, P_R	Corr. coef. R	0.977	0.734	0.702	0.647	0.548	0.431
	Exponent	0.62	0.38	0.349	0.37	0.25	0.17
	Constant A	401	1943	469	546	208	89
Ultimate resilience, U	Corr. coef. R	0.995	0.76	0.733	0.571	0.444	0.341
	Exponent n	0.59	0.41	0.38	0.357	0.22	0.15
	Constant A	904	3713	862	785	239	96
Strain energy, Se	Corr. coef. R	0.996	0.971	0.955	0.94	0.874	0.837
	Exponent n	0.816	0.737	0.695	0.65	0.49	0.41
	Constant A	1568	8945	2037	1743	540	231

*All correlations were carried out using the units of erosion rate as mm^3/kg.

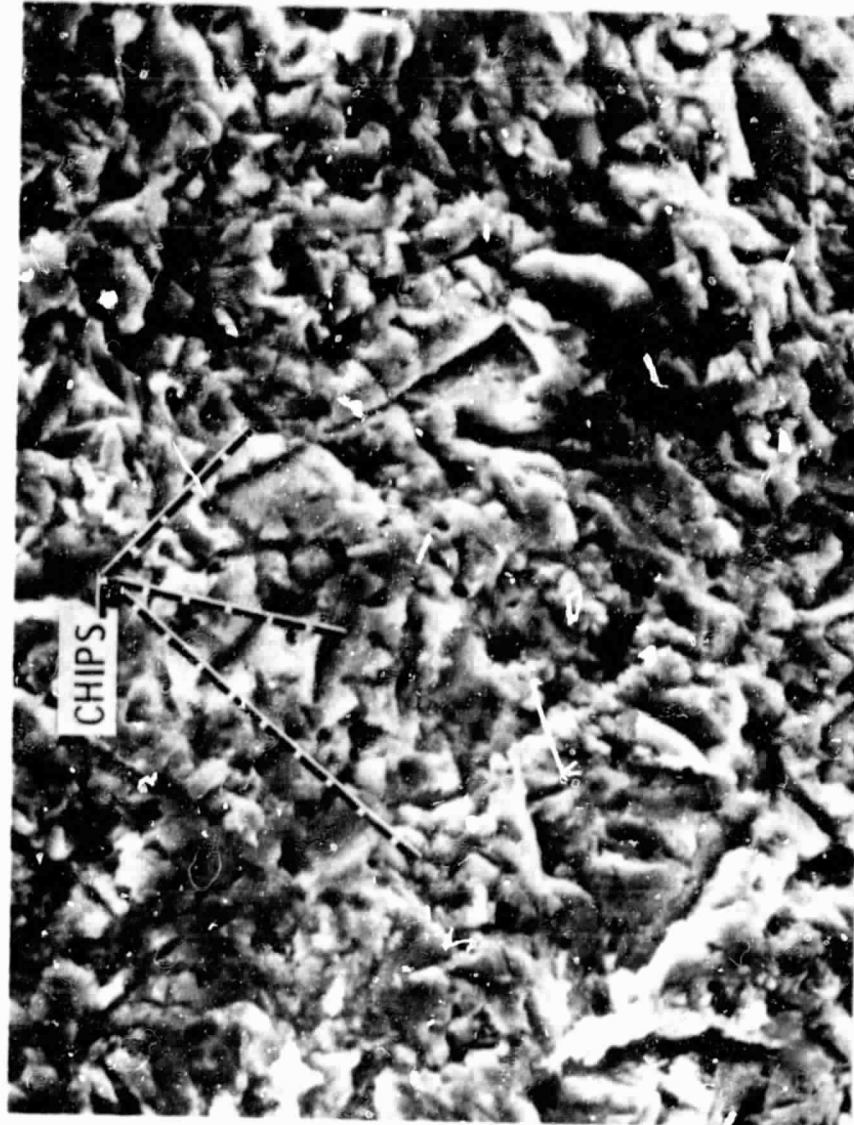TABLE 3. - CORRELATIONS OF MATERIAL PROPERTIES WITH SOLID PARTICLE EROSION*

[Erosion rate = A/(material property)^n. V = particle velocity; θ = angle of impingement; α = coefficient of expansion; K = bulk modulus; $\Delta T = T_m - T_{atm}$; T_m = melting point; T_{atm} = temperature of specimen; C_p = specific heat at constant pressure; ρ = density.]

Property	Parameter	Tadolder [21] data; quartz sand; V = 82 m/s; θ = 45°	Finnie, et al. [3] data; SiC (250 μm size)				
			V = 136 m/s; θ = 20°	V = 76 m/s; θ = 20°	V = 76 m/s; θ = 30°	V = 76 m/s; θ = 50°	V = 76 m/s; θ = 90°
Surface energy	Constant A	141	988	256	230	126	73
	Exponent n	1.77	1.50	1.42	1.26	1.00	0.92
	Corr. coef. R	0.965	0.965	0.957	0.981	0.946	0.934
Hardness	Constant A	1284	9920	2405	2.83×10^3	1332	766
	Exponent n	0.76	0.74	0.71	0.71	0.60	0.54
	Corr. coef. R	0.985	0.910	0.844	0.844	0.697	0.552
Melting point	Constant A	1.87×10^5	1.68×10^6	3.96×10^5	7.04×10^5	2.09×10^5	9.91×10^4
	Exponent n	1.17	1.16	1.14	1.20	1.07	1.01
	Corr. coef. R	0.956	0.933	0.923	0.905	0.789	0.659
Elastic modulus	Constant A	1.29×10^4	9.74×10^4	2.20×10^4	1.82×10^4	5.93×10^3	2.74×10^3
	Exponent n	1.14	1.09	1.06	1.01	0.83	0.73
	Corr. coef. R	0.898	0.885	0.871	0.824	0.666	0.519
Bulk modulus	Constant A	7.42×10^4	3.33×10^5	8.03×10^4	7.38×10^4	2.67×10^4	1.37×10^4
	Exponent n	1.51	1.35	1.34	1.32	1.17	1.09
	Corr. coef. R	0.942	0.937	0.936	0.905	0.782	0.647
Coefficient of thermal expansion	Constant A	2.88×10^8	3.18×10^8	6.41×10^7	1.34×10^8	2.50×10^6	9.45×10^4
	Exponent n	-1.38	-1.18	-1.15	-1.19	-0.87	-0.61
	Corr. coef. R	-0.831	-0.652	-0.641	-0.652	-0.464	-0.288
Cohesive energy	Constant A	1.43×10^5	3.26×10^6	7.28×10^5	5.62×10^5	1.02×10^5	3.05×10^4
	Exponent n	1.33	1.45	1.44	1.39	1.15	0.99
	Corr. coef. R	0.746	0.765	0.766	0.768	0.636	0.477
Atomic volume	Constant A	2.04×10^6	7.42×10^7	1.41×10^7	5.21×10^8	1.75×10^8	1.75×10^8
	Exponent n	-2.28	-2.57	-2.52	-3.37	-3.20	-3.35
	Corr. coef. R	-0.754	-0.873	-0.863	-0.861	-0.798	-0.744
Metal-metal bond energy	Constant A	3.58×10^6	7.57×10^4	1.74×10^4	2.21×10^4	4.60×10^3	1.14×10^3
	Exponent n	1.50	1.11	1.10	1.11	0.82	0.57
	Corr. coef. R	0.822	0.640	0.638	0.653	0.473	0.291
$C_p \Delta T$	Constant A	7.63×10^2	5.13×10^3	3.58×10^9	2.04×10^{10}	1.12×10^9	1.08×10^8
	Exponent n	0.863	0.71	0.71	0.779	0.67	0.59
	Corr. coef. R	0.897	0.819	0.828	0.827	0.696	0.539
αKΔT (Coefficient of thermal expansion x bulk modulus x temperature differential)	Constant A	87.18	7.4×10^2	1.98×10^2	1.99×10^2	1.42×10^2	1.05×10^2
	Exponent n	1.04	0.93	0.92	0.98	0.93	0.94
	Corr. coef. R	0.971	0.991	0.989	0.978	0.906	0.808
Ultimate resilience x hardness	Constant A	1.06×10^3	5.9×10^3	1.33×10^3	9.68×10^2	2.90×10^2	1.22×10^2
	Exponent n	0.336	0.303	0.284	0.257	0.176	0.139
	Corr. coef. R	0.999	0.990	0.982	0.950	0.894	0.829
(Debye temperature)^2 x atomic weight	Constant A	1.27×10^{11}	9.52×10^{11}	1.74×10^{11}	2.12×10^{11}	5.65×10^9	4.54×10^8
	Exponent n	1.35	1.34	1.31	1.32	1.11	0.97
	Corr. coef. R	0.827	0.852	0.842	0.841	0.692	0.536

*All correlations were carried out using the units of erosion rate as mm^3/kg.
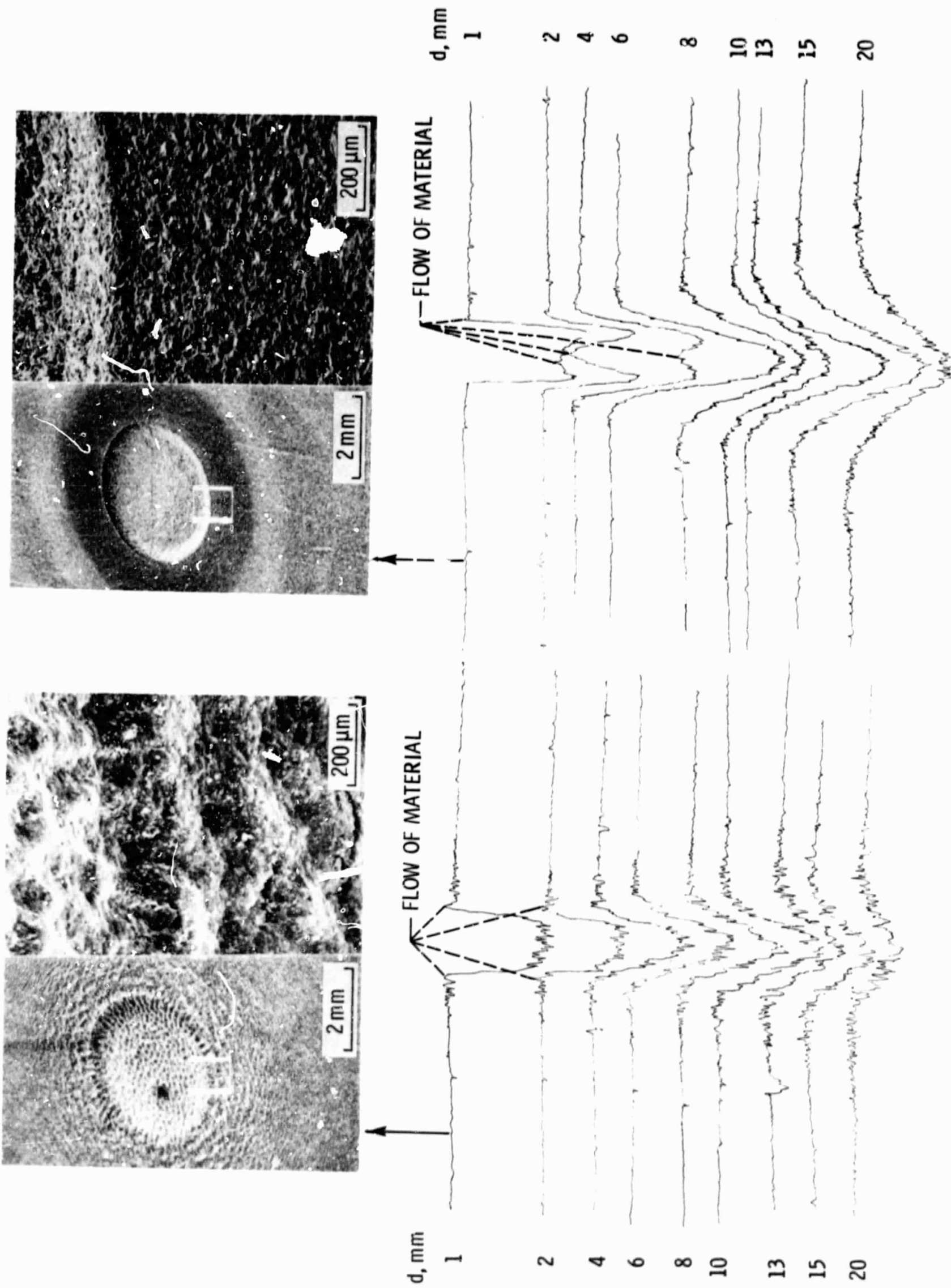
(b) Jagged, angular craters and cut surfaces with chips due to angular particle impingement (cutting wear).

(a) Flake like wear debris due to glass bead impingement (deformation wear).

Figure 1. - Wear debris during spherical and angular particle impingement erosion.

(a) Glass bead impingement (V = 87 m/s).

(b) Crushed glass impingement (V = 87 m/s).

Figure 2. - Surface traces during incubation period as a function of the distance of the nozzle above the specimen surface.
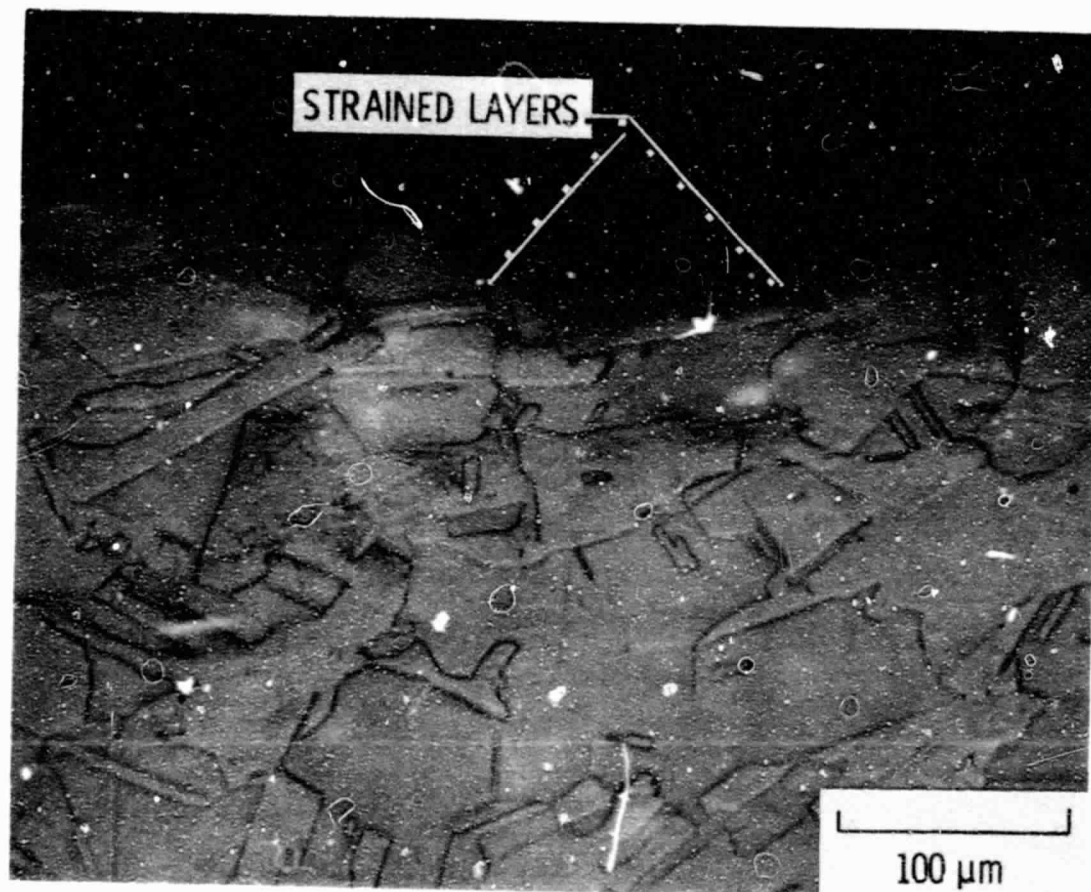
Figure 3. - Photograph showing strained layers on pure copper sur-
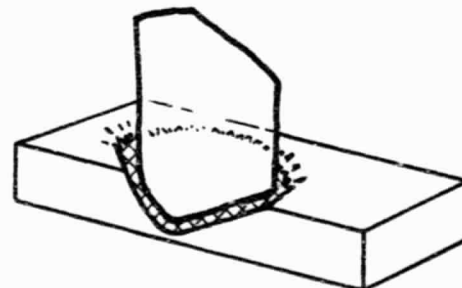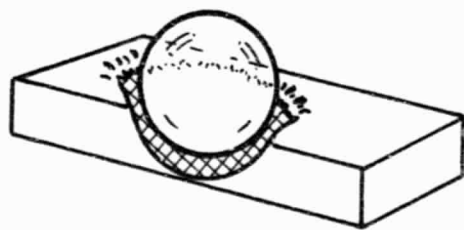face during glass bead impingement.
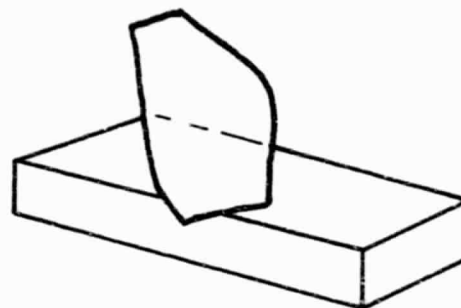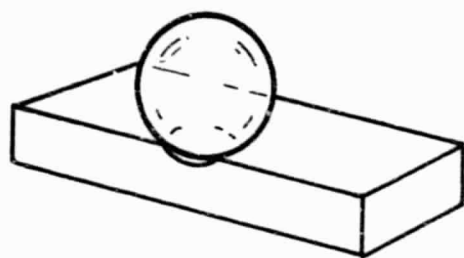
ELASTIC DEFORMATION
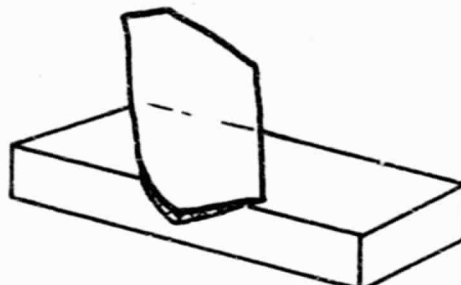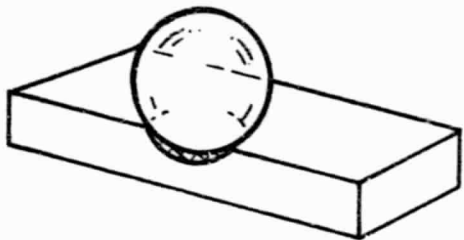
PLASTIC DEFORMATION
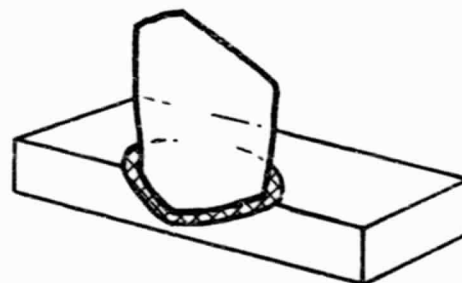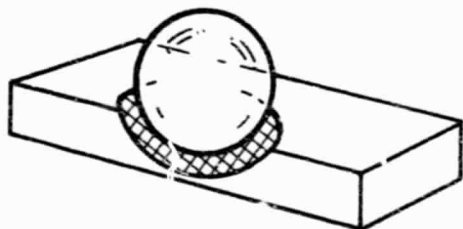
PLASTIC FLOW AND LIP FORMATION

EXTRUSION OF MATERIAL AND MELTING

(a) Spherical particle impingement.

(b) Angular particle impingement.

Figure 4. - Different forms of failure modes during solid particle impingement.
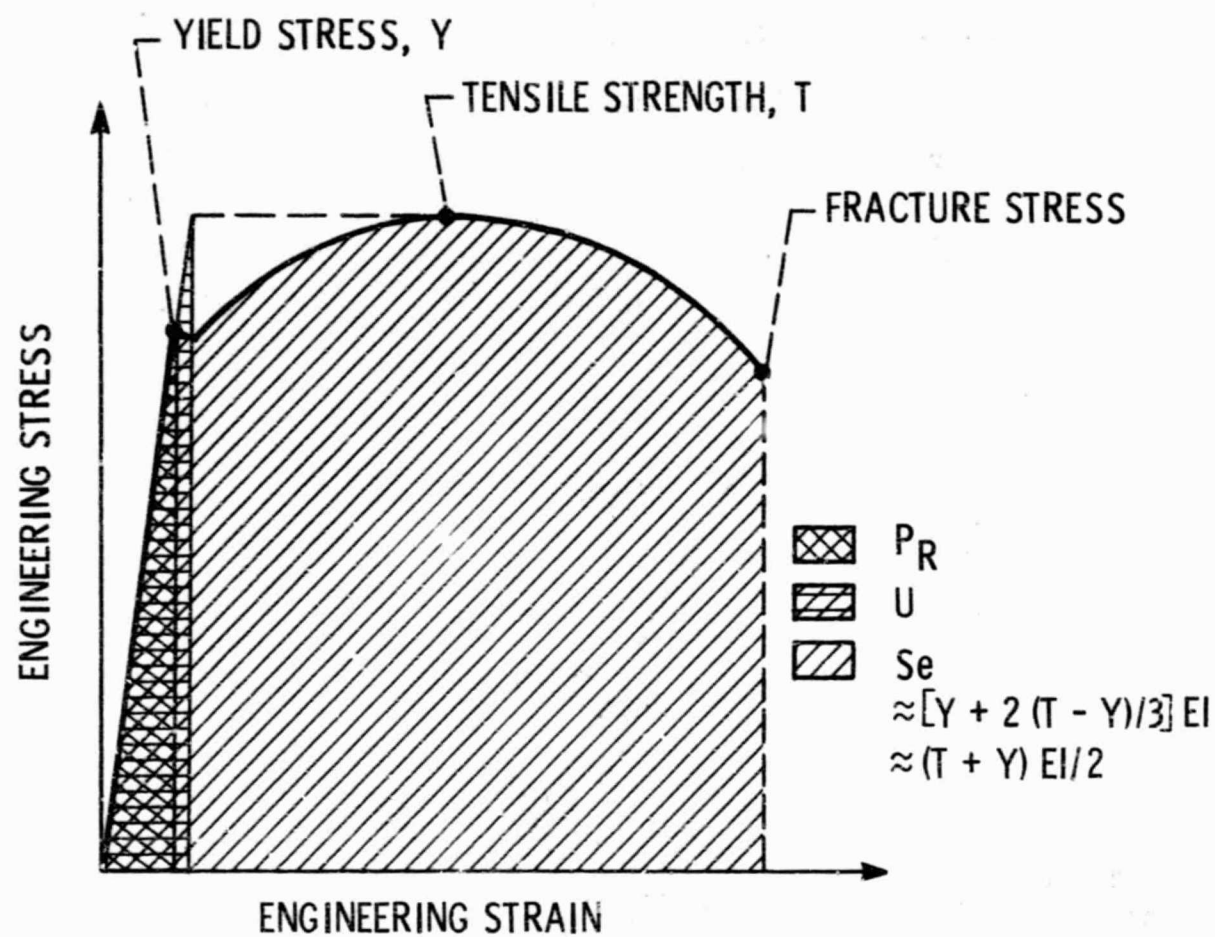
Figure 5. - Engineering stress-strain diagram explaining the concepts of energy absorption characteristics. Proof resilience, P_R =[yield stress]^2/[2 x elastic modulus]. Ultimate resilience, U =[tensile strength]^2/[2 x elastic modulus]. Strain energy (work done to cause failure), S_e = area under the stress-strain curve.

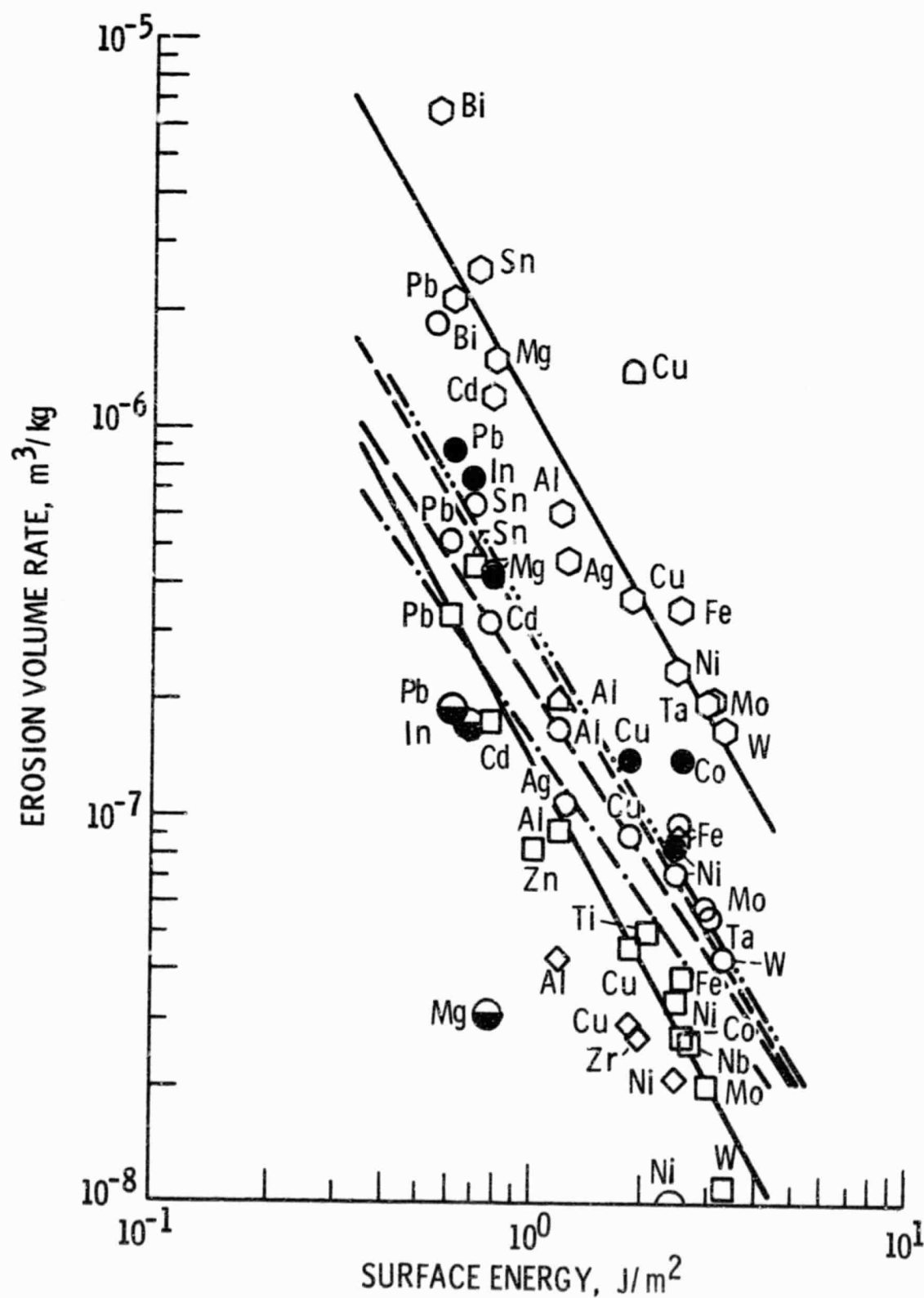|	V, m/s	ERODENT	SIZE, μm	ANGLE, deg	REF.
—⬡—	137	SiC	250	20	[3]
—◯--	76	SiC	250	20	[3]
– – –	76	SiC	250	30	[3]
–·–·	76	SiC	250	50	[3]
–··–	76	SiC	250	90	[3]
△	410	SiO$_2$	400	--	[4]
⬠	305	QUARTZ	40	--	[8]
◇	66	OLIVINE SAND	350–500	45	[48]
—☐—	82	SiO$_2$	---	45	[21]
⊖	170	Al$_2$O$_3$	27	90	[49]
●	68	CRUSHED GLASS	30	90	THIS STUDY
⬗	101	GLASS BEADS	20	90	THIS STUDY

Figure 6. - Erosion rates of different metals as a function of surface energy.

	V, m/s	ERODENT	SIZE, μm	ANGLE, deg	REF.
—⬡—	137	SiC	250	20	[3]
—○—	76	SiC	250	20	[3]
- - -	76	SiC	250	30	[3]
—·—	76	SiC	250	50	[3]
—··—	76	SiC	250	90	[3]
△	410	SiO₂	400	--	[4]
◨	305	QUARTZ	40	--	[8]
◇	66	OLIVINE SAND	350-500	45	[48]
—▱—	82	SiO₂	---	45	[21]
⊖	170	Al₂O₃	27	90	[49]
●	68	CRUSHED GLASS	30	90	THIS STUDY
⊖	101	GLASS BEADS	20	90	THIS STUDY

Figure 7. - Erosion rates of different metals as a function of atomic volume.

	V, m/s	ERODENT	SIZE, μm	ANGLE, deg	REF.
—○—	137	SiC	250	20	[3]
—○—	76	SiC	250	20	[3]
— — —	76	SiC	250	30	[3]
—·—	76	SiC	250	50	[3]
—··—	76	SiC	250	90	[3]
△	410	SiO₂	400	--	[4]
⬠	305	QUARTZ	40	--	[8]
◇	66	OLIVINE SAND	350-500	45	[48]
—□—	82	SiO₂	---	45	[21]
⊖	170	Al₂O₃	27	90	[49]
●	68	CRUSHED GLASS	30	90	THIS STUDY
◑	101	GLASS BEADS	20	90	THIS STUDY

Figure 8. - Erosion rates of different metals as a function of melting point.

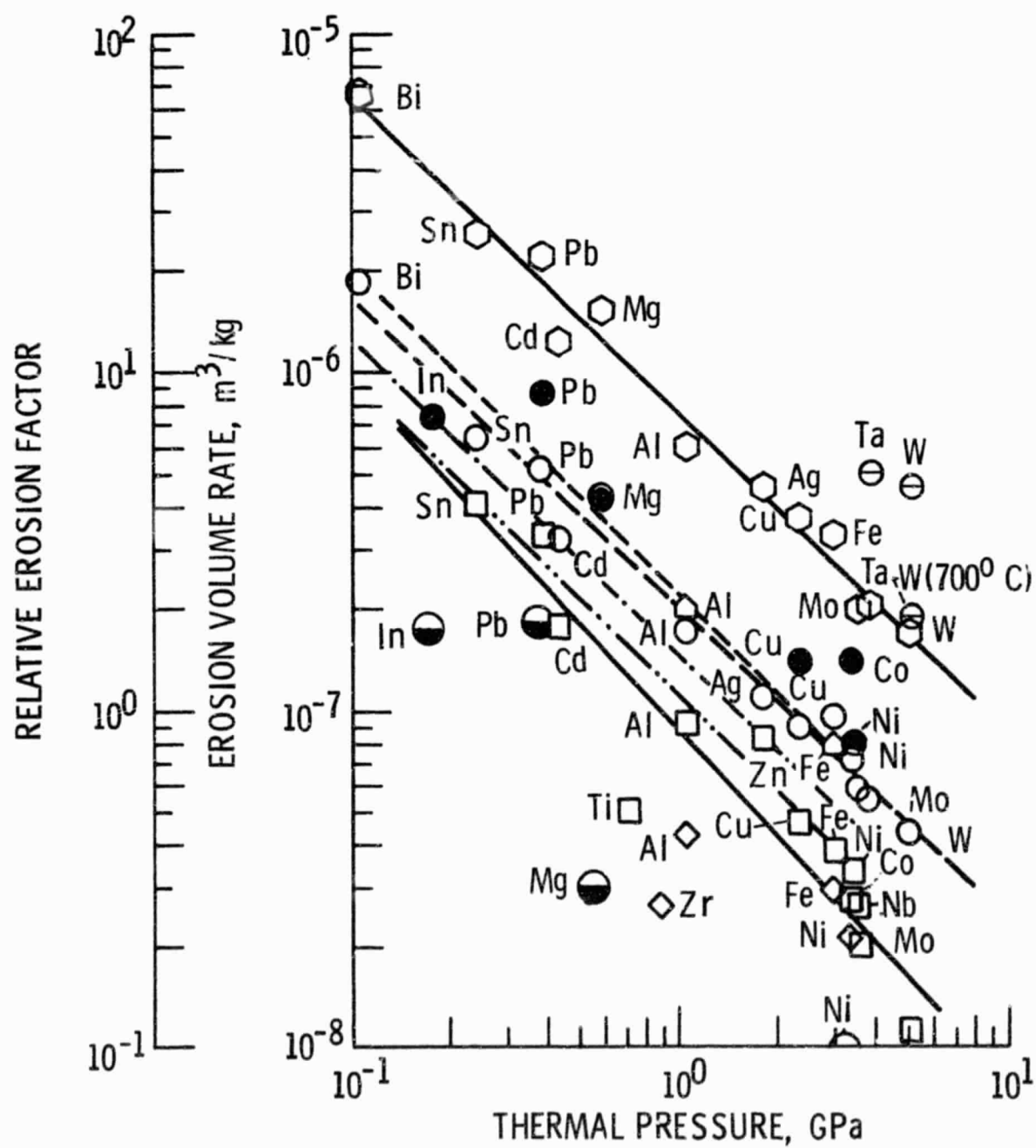|	V, m/s	ERODENT	SIZE, μm	ANGLE, deg	REF.
—⬠—	137	SiC	250	20	[3]
—○—	76	SiC	250	20	[3]
— — —	76	SiC	250	30	[3]
—·—·—	76	SiC	250	50	[3]
—··—··—	76	SiC	250	90	[3]
△	410	SiO$_2$	400	--	[4]
◻	305	QUARTZ	40	--	[8]
◇	66	OLiVINE SAND	350-500	45	[48]
—□—	82	SiO$_2$	---	45	[21]
⊖	170	Al$_2$O$_3$	27	90	[49]
●	68	CRUSHED GLASS	30	90	THIS STUDY
◑	101	GLASS BEADS	20	90	THIS STUDY

Figure 9. - Erosion rates of different metals as a function of thermal pressure.